J. Appl. Comput. Mech., 7(1) (2021) 334-344
DOI: 10.22055/JACM.2020.35246.2607

ISSN: 2383-4536
jacm.scu.ac.ir

Shahid Chamran University of Ahvaz

Journal of Applied and Computational Mechanics

Research Paper

Constructal Design of an Idealize Arterial Bypass Graft: Effect of the Bypass Attachment Pointon Resistance to Flow

Andrea Natale Impiombato[1], Flavia Schwarz Franceschini Zinani[2], Luiz Alberto Oliveira Rocha[2], Cesare Biserni[1]

[1] Department of Industrial Engineering (DIN), School of Engineering and Architecture, Alma Mater Studiorum – University of Bologna, Viale Risorgimento 2, 40136 Bologna, Italy
[2] Mechanical Engineering Graduate Program, Universidade do Vale do Rio dos Sinos, 93022-750 São Leopoldo, Brazil

Received October 01 2020; Revised November 04 2020; Accepted for publication November 04 2020.
Corresponding author: Andrea Natale Impiombato (andrea.impiombato2@unibo.it)

Abstract. This paper aims to investigate, through the 3D numerical analysis of an idealized arterial bypass graft, the dependence of the resistance to flow on the bypass insertion point. The computational model assumes a laminar steady-state Newtonian fluid flow and three different Reynolds numbers: 150, 250, and 400. In this study, the constructal theory has been employed, a self-standing law in physics which covers the statement of minimum flow resistance to optimize morphing architectures, i.e. the coronary artery bypass grafting. According to the Constructal Design method, the constraints are stenosis degree, junction angle, and diameter ratio, while the attachment point is defined as a design parameter. The results demonstrate that the distance between the bypass attachment point and the stenosis influences the pressure drop; more specifically, the pressure drop decreases with the augmentation of the distance. In this regard, a different distribution of the mass flows between the bypass, and the artery is observed and seemed to be the main reason for that behavior. The application of the Constructal Design method in hemodynamics is a tool to describe the biological system to search for better flow performance since it is based on the natural evolution of living systems.

Keywords: Constructal Design; Blood flow; Coronary artery; Bypass graft; Dimensionless pressure drop.

1. Introduction

Arteriosclerosis is a tissue hardening, or sclerosis, of the arterial wall that appears with age as a consequence of the accumulation of fibrous connective tissue at the expense of the elastic component [1]. Tian at al. [2] and Liu et al. [3] explain that the main manifestations of atherosclerosis are stenoses, or the formation of atherosclerotic plaques on the internal wall of the arteries with consequent narrowing of the lumen, and aneurysms, or the loss of elasticity of the wall of a vessel that involves distension. According to Guerciotti et al. [4], one type of surgery, for people with high risk, is the coronary artery bypass graft (CABG) innest. The surgical procedure consists of bypassing a stenotic region to restore the heart's blood flow. Intimal hyperplasia (IH) is the principal factor that affects graft patency. An anomalous production of smooth muscle cells arises between the graft and the coronary artery instigating a reduction of the lumen of the graft and the consequent restenosis and obstruction of the graft [5]. The science of computational fluid dynamics (CFD) has been applied extensively to explore the connection between hemodynamics in CABGs and IH development and assist in the improvement of a top graft design. Bertolotti and Deplano [6] used a three-dimensional numerical model with different stenosis positions relative to the downstream junction. They concluded that the risks of intimal hyperplasia at the anastomosis might be reduced by increasing the distance between the stenosis and the junction. Lee et al. [7] studied the flow behavior of a complete bypass graft and a 100% occluded artery with different Reynolds number and junction angles. Vimmr et al. [8] implemented several numerical simulations of a complete three-dimensional coronary bypass model as a function of three geometrical parameters (stenosis degree, junction angle, and diameter ratio). They revealed that the diameter ratio was the most crucial parameter for coronary artery bypass grafting (CABG).

In Ref. [9], the stenosed coronary artery bypass graft including an analysis of the blood flow phenomena and wall shear stress, based on a three-dimensional computer model, was analyzed and developed to approach a realistic situation, inlet pulse and non-Newtonian behavior. The results demonstrated that the anastomosis of 45° was the most appropriate for resolving the coronary heart disease problem. Moreover, Ref. [10] is focused on the study of several configurations of patient-specific coronary artery bypass grafts while a specific design for coronary arterial bypass surgical grafting, consisting of coupled sequential side-to-side and end-to-side anastomoses, is treated in Ref. [11]. On the same topic, O'Callaghan et. al. [12] demonstrated that the choice of blood constitutive equation (among Newtonian, Carreau, Power law, Carreau–Yasuda, Bi-exponential, Cross, Modified Cross, Herschel–Bulkley, etc.) has to be based on the particular situation under study e.g. flow rate, steady/unsteady flow, and geometry. Additional interesting computations regarding coronary artery bypass grafting have been treated in Refs. [13,14].

Dutra et al. [15] applied the Constructal Design to investigate the effect of geometric parameters on the flow through a bypass

Published online: November 15 2020

graft circumventing an idealized, partially-stenosed coronary artery. They have discovered that at fixed flow conditions, the pressure drop is mitigated if the parameters assume a specifics values. The introduction of the Constructal Design method into the field of hemodynamics brings a valuable tool to the understanding of biological problems since the bypass geometry is known to affect the blood flow field significantly and to play an essential role in potential graft failure due to intimal hyperplasia.

The Constructal design method has been employed in various engineering sectors [16,17], and beyond, as a new approach for solving optimization problems. In general, according to Constructal Law, stated by Adrian Bejan in 1996, "for a finite-size flow system to persist in time (to live) it must evolve with freedom in such a way that it provides easier access to imposed currents that flow through it" [18]. Constructal Law deals with the physical concepts of life, evolution, design, performance, and time arrow [19]. Under Constructal Theory, evolution and design in nature are deterministic because the living systems evolve in such a way to decrease resistance to flow [20]. The growth of scientific research concerning Constructal Law has been documented in review articles [21-23] and books [18-20]. Constructal Design is the method that allows the mathematical modeling of flow systems evolution. It can explain the configuration of existing systems in nature and to design flow systems in engineering. This design methodology has the objectives of accessing the effects of shape and geometry in flow performance so that the optimal geometry may be discovered by means of a given optimization technique (exhaustive search or heuristic methods), according to Constructal Law [24]. The applications of Constructal Design cover many engineering fields such as heat and mass transfer, renewable energy, manufacture, and materials [24-28]. Until now, the few applications of Constructal Theory in medicine were within the field of cancer treatments, as studied by Wang et al. [27] and Lucia and Grisolia [28]. Therefore, taking into account the domain of coronary artery bypass grafting, this papers documents numerically, on the basis of Constructal design, the search for the length ratio that minimizes the dimensionless pressure drop for definite combinations of stenosis degree, junction angle, aspect ratio and Reynolds number. It is worth mentioning that no previous studies were found in literature specifically focused on the effect of the bypass attachment point.

2. Methodology

2.1 Constructal Design

Dutra at al. [15] have conducted a very detailed study on the application of the Constructal Design method to determine the system constraints and parameters. The evaluation of the constraints begins from the definition of the domain shown in Figure 1.

It is an idealized version of an artery partially obstructed and implanted with a symmetrical graft. The artery is represented as the host artery with a diameter equal to D and length equal to $L_1 + 2L_5$. The main tube undergoes stenosis that reduces its diameter D_0. The graft is placed at a distance L_2 from the center of the stenosis, and D_1 denotes its diameter. The junction angle is α, and the graft diameter is D_1. L_3 is the distance from the center at the tube starts to get narrow, i.e., it models the stenosis morphology. According to Ref. [15], the flow is incompressible and Newtonian. The inlet average velocity is Um, assessed by fixing the Reynolds Number. The tube walls are modeled as rigid, impermeable, and non-slip. The flow is also assumed to be three-dimensional, steady, incompressible, and laminar. It is worth mentioning that the hypothesis of steady state simulations is common in literature: see for example Refs. [29,30]. The inlet section was placed far from the stenosis ($L_5 = 25D$) to ensure that the flow arrives, at the bypass inlet, fully developed. Instead, the outlet section was also taken away from the stenosis (L_5) in such a way as to minimize the effect of imposing the constant outlet pressure value. Imposing a constant outlet pressure value is not realistic, but it is necessary to solve the equations in this case. For all simulations, the host artery diameter D is equal to 3 mm, corresponding to an average value of the right coronary artery [6, 15]. The system's characteristic volumes were defined in the following way [15], where the total artery volume V is considered without the narrowed:

$$V = \pi \frac{D^2}{4}(L_1 + 2L_5), \tag{1}$$

where D is the artery diameter and (L_1+2L_5) is the total artery length. The graft volume V_1 is

$$V_1 = \pi \frac{D_1^2}{4} L_4, \tag{2}$$

where D_1 is the graft diameter and L_4 is the total graft length. It is worth mentioning that the graft is not a straight cylinder with inlet/outlet normal to its axis. In this work, the value of V was fixed considering D = 3 mm, $L_1 = 50D$ and $L_5 = 30D$. Instead, the value of V_1 is not fixed because the length L_4 is a function of the bypass attached point position (L_2) and the junction angle α. The stenosis degree S is calculated as

$$S = \frac{D - D_0}{D} 100, \tag{3}$$

where D_0 is the diameter at the center of the stenosis.

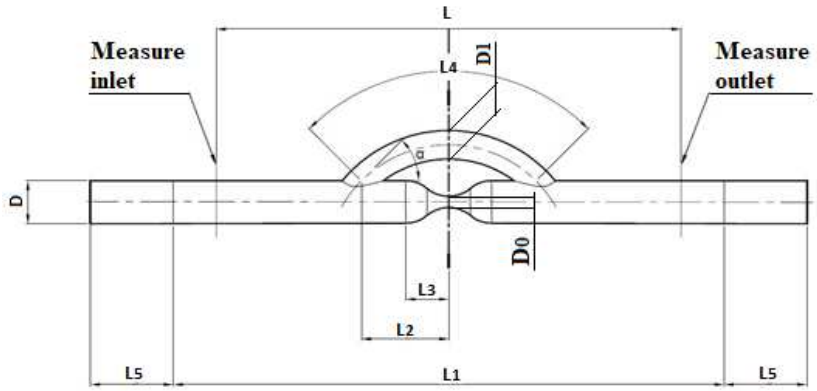

D	Artery Diameter
D_0	Stenosis Diameter
D_1	Bypass Diameter
L	Measuring Length
L_1	Bypass Region
L_2	Bypass Attachment Point
L_3	Stenisis Beginning
L_4	Bypass Length
L_5	Added Length
α	Bypass angle

Fig. 1. Problem domain.

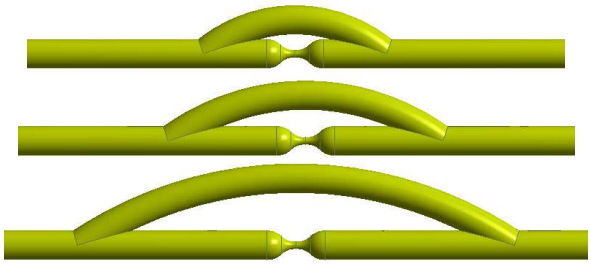

Fig. 2. Some different bypass graft configuration for L_2/D equal to 2.5 (top), 4 (middle) and 6.67 (bottom) at fixed bypass junction angle α = 30° and bypass diameter ratio D_1/D = 1.

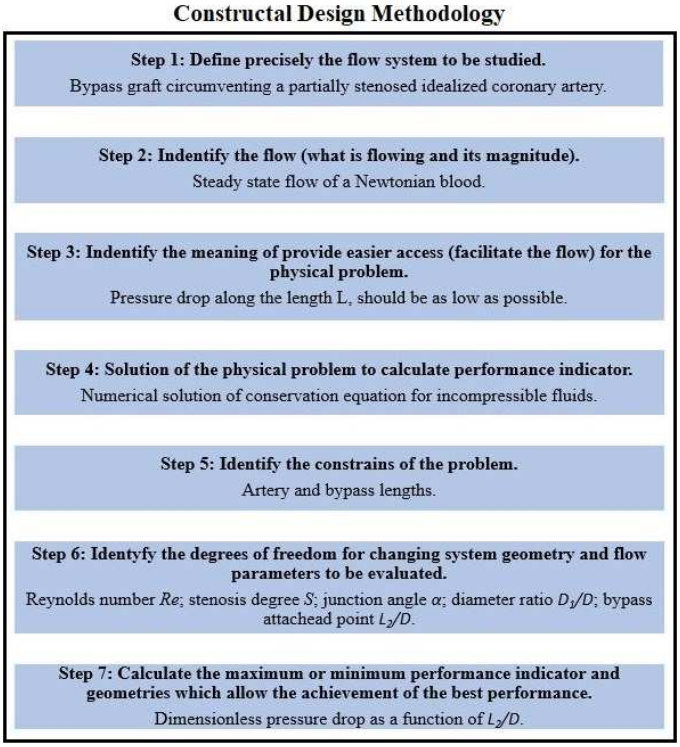

Fig. 3. Constructal design flowchart.

A baseline case from literature [8,15] was used for the definition of the values L_1/D = 16.67 and L_3/D=1. The value L_2/D is the parameter that is made to vary in the range $2.5 \leq L_2/D \leq 6.67$. Figure 2 shows the configuration for L_2/D equal to 2.5, 4 and 6.67. In Ref. [15] this parameter was fixed at 2.5 D. This means that considering D = 3mm, the value of L_2 was fixed at 7.5 mm. In this work L_2 varies from 7.5 mm to 20 mm.

At fixed bypass junction angle α (30°) and bypass diameter ratio D_1/D=1, two values of stenosis degree S (50% and 75%) were evaluated at three different Reynolds Numbers (150, 250 and 400). Blood is modelled as an incompressible Newtonian fluid with density ρ = 1000 kg/m^3 and dynamic viscosity μ = 0.0035 Pa s [31]. The assumption of blood as Newtonian fluid is acceptable and used by other studies in the hemodynamic area, e.g., Ko et al. [31], Ko et al. [32], Xiong and Chong [33] and Vimmr et al. [8]. The choice to keep $\alpha$and D_1/D fixed at the chosen values derives from the fact that it is interesting to investigate the effect over the pressure drop due to the bypass attachment point position. From previous studies [8, 15] it is known that an increase of α would cause a greater pressure drop while a decrease of αwould cause a lower pressure drop. With D_1/D values close to 1, the effect on the pressure drop improves significantly [8, 15].

Constructal Theory assumes that living systems evolve limited by space [22]. Accordingly, Constructal Theory systems must evolve to provide easier access to its flows [20]. To this end, it was considered that the dimensionless pressure drop $\tilde{p}$ (that will be defined in Eq. (6)) along the length L should be as low as possible. Thus, an optimization problem was formulated as in Ref. [15]: "Find the minimum $\tilde{p}$. The design variable is the length ratio L_2/D." Therefore, the degree of freedom for this problem is the diameter ratio L_2/D. A search is conducted for the length ratio L_2/D that minimizes the value of the pressure drop $\tilde{p}$ for specific combinations of S, α, D_1/D and Re. Figure 3 details all the steps required by the Constructal Design methodology.

2.2 Mathematical Modelling

The flow system is described by the mass and moment balance equations [15]:

$$\frac{\partial \tilde{u}_i}{\partial \tilde{x}_i} = 0 \tag{4}$$

$$\tilde{u}_i \frac{\partial \tilde{u}_i}{\partial \tilde{x}_j} = -\frac{\partial \tilde{p}}{\partial \tilde{x}_i} + \frac{1}{\mathrm{Re}} \frac{\partial \tilde{\tau}_{ij}}{\partial \tilde{x}_j} \tag{5}$$

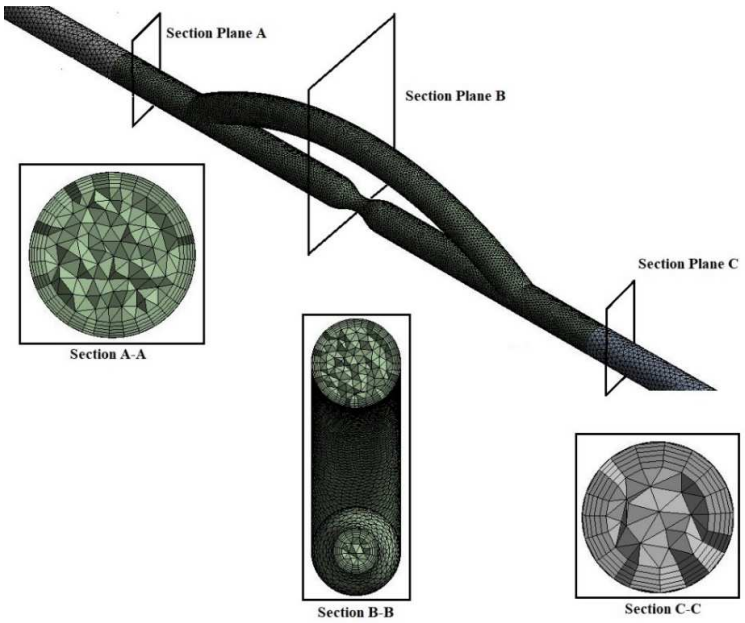

Fig. 4a. Computational mesh.

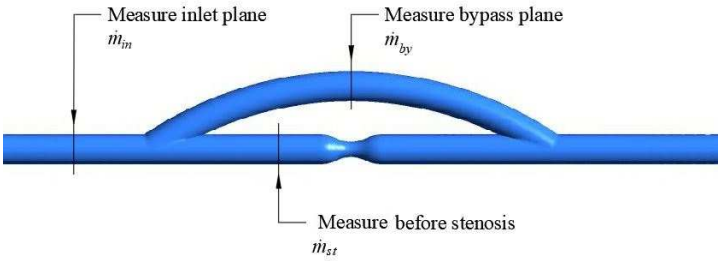

Fig. 4b. Plane measure.

where $\tilde{u}_i$ is the dimensionless velocity field, $\tilde{x}_i$ is the dimensionless position vector, $\tilde{p}$ is the dimensionless pressure drop, $\tilde{\tau}_{ij}$ is the dimensionless extra stress tensor field and Re is the Reynolds number defined as [15]:

$$\tilde{u}_i = \frac{u_i}{U_m}, \tilde{x}_i = \frac{x}{D}, \tilde{p} = \frac{\Delta p}{\rho U_m^2}, \tilde{\tau} = \frac{\tau_{ij}}{(U_m \mu)/D}, \mathrm{Re} = \frac{\rho U_m D}{\mu} \tag{6}$$

where U_m is the average velocity at the inlet, D is the diameter of the artery, ΔP is the pressure drop along L, ρ is the fluid mass density and μ is the fluid viscosity. The constitutive equation for the extra stress is that of a generalized Newtonian liquid [34,35]:

$$\tau_{ij} = 2\eta(\dot{\gamma}) D_{ij} \tag{7}$$

where $\eta(\dot{\gamma})$ is the viscosity function and D_{ij} is the strain rate tensor, given as the symmetric part of the velocity gradient tensor [35]. For a Newtonian fluid, $\eta(\dot{\gamma})$ is a constant and equal to μ [35]. For the simulation it was considered a Newtonian blood as working fluid. The physical properties and parameters used for the dimensioning of Eqs. (4)-(5), according to rules (6), are ρ=1000 kg/m^3 and μ=0.0035 Pa s.

2.3 Numerical Method and Computational Grid

Using ANSYS/FLUENT v. 18.2 [36], the Finite Volume Method [37] was employed to solve the partial differential equation system. A pressure-based solver was used with a pressure-velocity coupling method, second-order interpolation functions for velocity fields, and linear interpolation function for the pressure field. All calculations were conducted in a double-precision representation of real numbers. The iterative algorithm was a false transient. The mesh was parameterized to keep the element sizes proportional according to the stenosis configuration and diameter ratio studied. Figure 4a shows the division of the domain.

The inlet and outlet ducts are discretized with tetrahedral finite elements with size 5.5×10^{-4} m. Instead, the area of interest was discretized with smaller tetrahedral finite elements having size 3.0×10^{-4} m. Along the walls, prismatic layers elements were used to capture the boundary layer better. Figure 4a presents a sample of the computational mesh for the model with detailed views at the cross-section in the different zone of the domain. As a convergence criterion scaled residuals of each equation at an iteration were used and compared with a user-defined convergence criterion equal to 10^{-6} for velocity and pressure fields. The Grid Convergence Index (GCI) method was applied for different values of Reynold number Re and length junction L_2/D at two values of stenosis degree S (50%, and 75%). As explained by Celik et al. [38], this method is useful for calculation and reporting of discretization error estimated in CFD simulations where experimental data may not be available for comparison. Table 1 and Table 2 summarize these results for S = 50% and S = 75% respectively. N_i represents the number of elements. It can be verified that the maximum GCI index was 2.36% using a refining mesh of a 30% factor. It is important to observe that, based on experience and not on formal derivation, a maximum GCI value of 5% is considered acceptable for this method [38]. The method to evaluate the pressure drop ΔP is explained in Section 2.4.

Table 1. Grid Convergence Index (GCI) for S = 50 %, α = 30° and D_1/D = 1 (with D = 3 mm).

		Case 1	Case 2	Case 3	Case 4	Case 5	Case 6	Case 7
	L_2/D	2.50	2.67	3.33	4.00	5.00	6.00	6.67
	N_1	259310	262360	276020	286970	304790	114870	118950
	N_2	156580	158630	164620	170220	179030	73428	75842
	N_3	105150	106960	110460	113490	118560	50887	52255
Re=150	ΔP_{N1} [Pa]	109.55	109.46	106.73	102.42	98.09	91.71	87.41
	ΔP_{N2} [Pa]	109.39	109.40	106.86	103.30	97.87	91.48	87.16
	ΔP_{N3} [Pa]	109.52	109.53	106.96	103.48	98.04	91.79	87.48
	GCI %	0.80	0.060	0.58	0.29	0.97	0.91	1.30
Re=250	ΔP_{N1} [Pa]	202.39	200.07	197.79	191.77	182.89	171.38	162.02
	ΔP_{N2} [Pa]	201.93	200.11	197.24	191.18	182.27	171.08	162.02
	ΔP_{N3} [Pa]	202.15	200.42	196.86	191.82	182.63	171.10	161.81
	GCI %	0.27	0.0040	0.86	0.50	0.60	0.017	4.17×10^{-7}
Re=400	ΔP_{N1} [Pa]	367.90	367.90	356.99	349.56	336.80	318.20	302.45
	ΔP_{N2} [Pa]	367.98	366.61	356.46	347.82	335.10	316.68	300.97
	ΔP_{N3} [Pa]	366.87	364.96	35640	348.62	335.38	316.74	301.19
	GCI %	0.0023	1.81	3.67×10^{-6}	0.54	0.13	0.027	0.11

Table 2. Grid Convergence Index (GCI) for S = 75 %, α = 30° and D_1/D = 1 (with D = 3 mm).

		Case 1	Case 2	Case 3	Case 4	Case 5	Case 6	Case 7
	L_2/D	2.50	2.67	3.33	4.00	5.00	6.00	6.67
	N_1	258330	261020	273360	285660	303880	321410	333890
	N_2	156090	157110	163950	170180	178670	187930	194740
	N_3	104770	92633	110070	113380	116550	121490	125240
Re=150	ΔP_{N1} [Pa]	118.50	119.20	118.13	117.24	115.87	114.00	112.38
	ΔP_{N2} [Pa]	118.58	119.39	118.19	117.31	116.09	114.31	112.90
	ΔP_{N3} [Pa]	118.70	119.69	118.22	117.84	116.54	114.75	113.02
	GCI %	0.17	0.34	0.064	0.011	0.23	0.81	0.17
Re=250	ΔP_{N1} [Pa]	220.58	219.39	221.67	219.44	218.77	217.09	214.24
	ΔP_{N2} [Pa]	219.85	221.87	221.58	219.18	218.63	216.93	215.00
	ΔP_{N3} [Pa]	219.97	22.75	221.94	219.97	219.13	216.50	214.36
	GCI %	0.081	0.018	0.017	0.073	0.031	0.055	2.36
Re=400	ΔP_{N1} [Pa]	407.32	402.57	405.40	403.72	403.98	408.43	407.32
	ΔP_{N2} [Pa]	405.12	407.88	405.05	403.85	402.66	405.36	406.71
	ΔP_{N3} [Pa]	403.98	408.40	406.66	404.33	405.83	406.45	406.01
	GCI %	0.73	0.18	0.030	0.015	0.29	0.52	1.27

Table 3. Grid Convergence Index (GCI) stenosis artery.

		S=50%	S=75%
	N_1	318440	417500
	N_2	185110	234950
	N_3	118740	153360
Re=150	$\Delta P_{N1,0}$ [Pa]	286.61	4745.40
	$\Delta P_{N2,0}$ [Pa]	286.94	4739.95
	$\Delta P_{N3,0}$ [Pa]	288.85	4738.83
	GCI %	0.030	0.037
Re=250	$\Delta P_{N1,0}$ [Pa]	627.61	11791.00
	$\Delta P_{N2,0}$ [Pa]	622.31	11780.35
	$\Delta P_{N3,0}$ [Pa]	622.49	11420.80
	GCI %	0.037	0.0034
Re=400	$\Delta P_{N1,0}$ [Pa]	1300.30	27750.00
	$\Delta P_{N2,0}$ [Pa]	1301.10	27690.35
	$\Delta P_{N3,0}$ [Pa]	1302.00	27680.98
	GCI %	0.62	0.050

In Table 3 the GCI index for geometry without bypass is analyzed with the aim of comparing the results of the different geometries. The mesh with the identical elements size was applied at the artery graft without bypass for evaluating the pressure drop on the same length and compare the results.

2.4 Procedure

Figure 4b shows the planes position where the pressure inlet P_{in} and pressure outlet P_{out} measurements were taken. The measurements planes have been positioned symmetrically concerning the shrinkage point. The distance L has been defined at 50 mm, or equivalent L/D=16.67. The L dimension remains fixed for all simulations. Once the pressure values have been obtained, the pressure drop ($\Delta p/L$) has been calculated as:

$$\left(\frac{\Delta P}{L}\right) = P_{in} - P_{out} \tag{8}$$

After that, the values calculated according to Eq. (8) have been compared with the pressure drop due without the bypass computed in the same way, obtaining the dimensionless quantity:

$$\tilde{p} = \frac{(\Delta p / L)}{(\Delta p / L)_0} \tag{9}$$

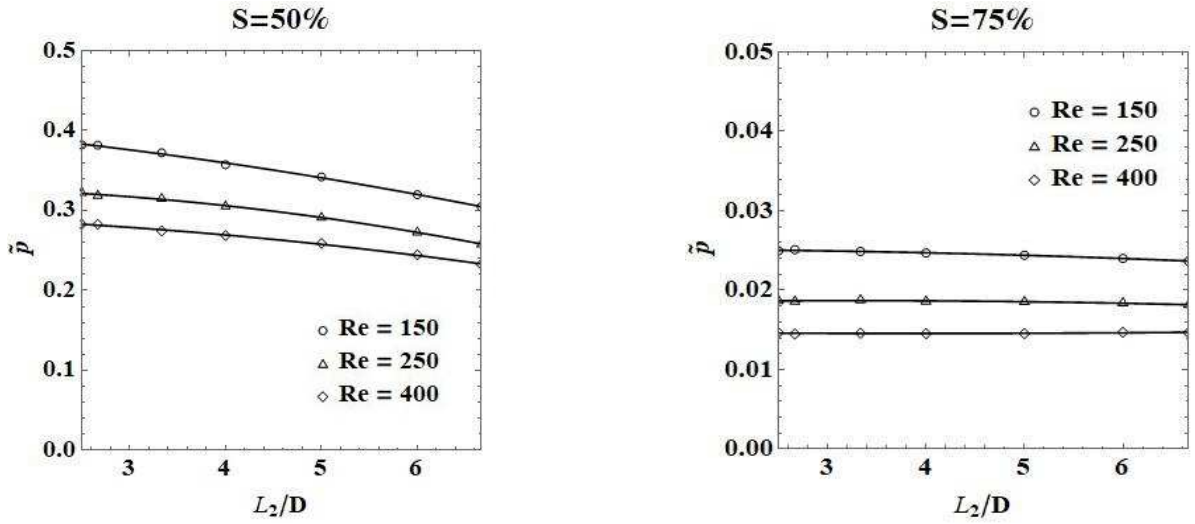

Fig. 5. Comparison of dimensionless pressure drop trend for S=50% (left) and S=75% (right) at different Reynolds Number Re.

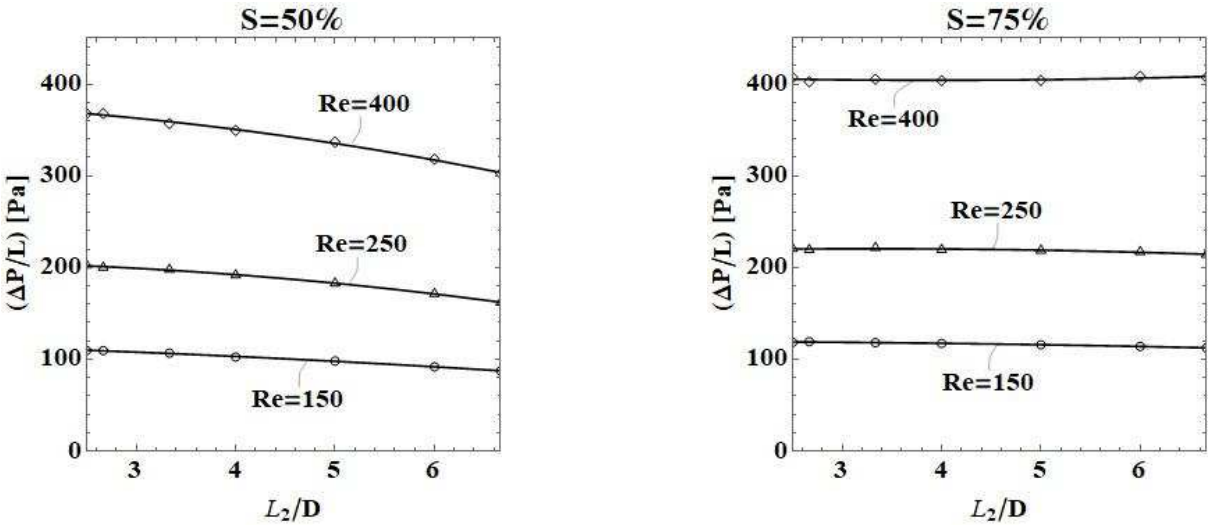

Fig. 6. Comparison of dimensional pressure drop trend for S=50% (left) and S=75% (right) at different Reynolds Number Re.

3. Results and Discussion

Figures 5 and 6 show the pressure drop as a function of the degree of freedom L_2/D with range $2.50 \leq L_2/D \leq 6.67$. Each curve represents the results of stenosis degree S equal to 50% and 75% at Reynolds Number Re equal to 150, 250, and 400.

The results show a monotonically decreasing trend for the pressure drop with increasing the distance of the bypass connection point L_2. This effect is significantly affected by the velocity of the fluid. When the Reynolds Number Re increases, the pressure drop follows the same trend of the other Reynolds numbers, but the magnitude of $\tilde{p}$, or (⊠p/L), decreases. The stenosis S value has an important effect on the pressure drop. The pressure mitigation effect with the bypass attachment point is less evident when S = 75%. Its trend remains approximately constant for each Reynolds values. To understand better the beneficial effect of the bypass, the mass flux in the different areas of the system was assessed. Table 4 and Table 5 are referred to Figure 7 and show the mass flow rate for S = 50% and S = 75% respectively.

The stenosis section was considered before the actual stenosis zone to be able to compare all mass flow rate with the other sections since the diameter remains equal to D.

As Reynolds Number Re increases, the mass flow rate is distributed in an increasingly different way, favoring the passage in the bypass section. This effect is more marked when the stenosis S increases. The mass flow rate through the bypass represents approximately 65-70% of the total mass flow rate. Knowing the mass flow rate values in the different bypass sections, it was possible to evaluate the resistances to the passage of fluid, due to the relation

$$R = \frac{\Delta p}{\dot{m}}, \tag{10}$$

where the resistance R is evaluated in [Pa s/kg] in S.I. It is worth mentioning that, with reference to Fig.1., the resistance is evaluated between the outlet and inlet measure plane.

Table 6 and Table 7 show the evaluations of the resistance R in the stenosis and bypass sections for S values 50% and 75% respectively. The graphical results form of Table 6 and Table 7 is represented in figure 8. The flow resistance decreases monotonically with increasing L_2. In particular, the stenotic resistance undergoes a considerable decrease with the increase of the bypass attachment point.

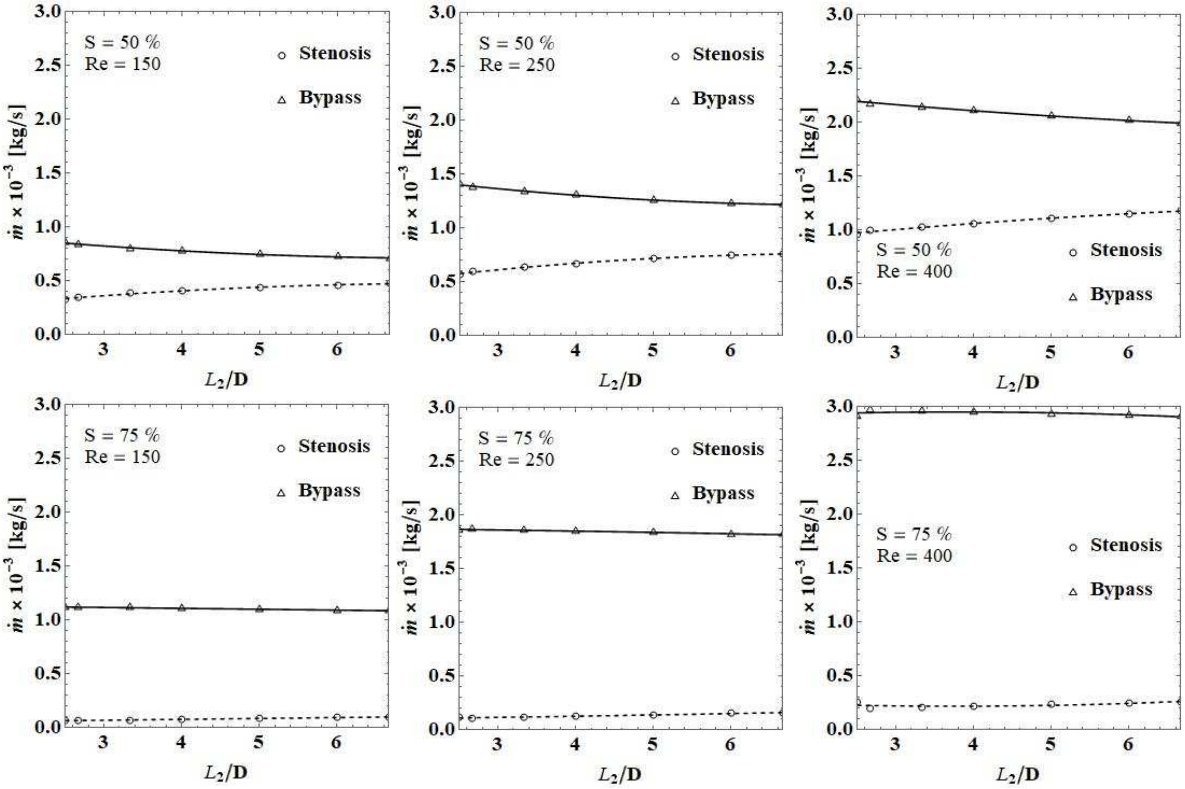

Fig. 7. Mass flow rate for S = 50% (top: Table 4) and S = 75% (bottom: Table 5).

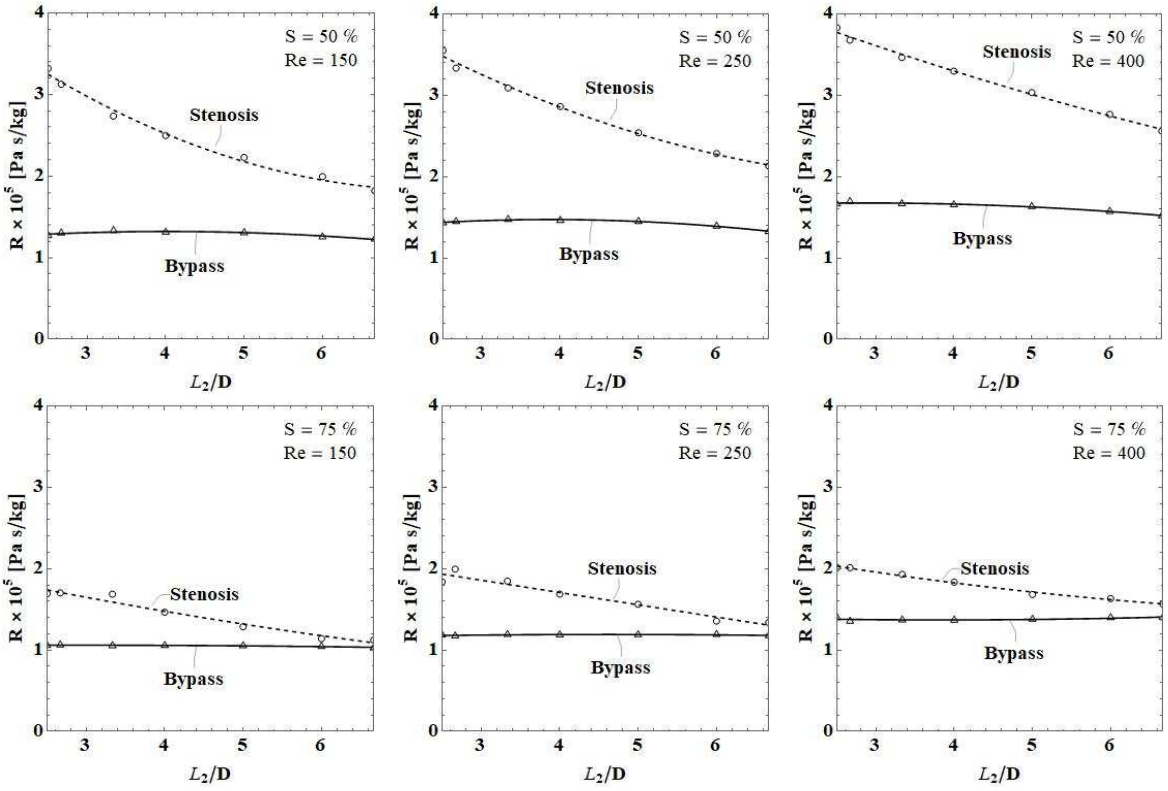

Fig. 8. Resistance R for S = 50% (top: Table 6) and S = 75% (bottom: Table 7).

Finally, Figure 9 illustrates velocity contours and streamlines with reference to a couple of outcome results. Please note the optimal configuration depicted on the right, having the following coordinates: L_2/D=6.67, S=75%, and Re=150.

Table 4. Evaluation of the mass fluxes in the measure inlet section ($\dot{m}_{in}$) stenosis section ($\dot{m}_{st}$) and central bypass section ($\dot{m}_{by}$) for S = 50 %, α = 30° and D_1/D = 1 (with D = 3 mm).

		Re=150, $\dot{m}_{in}$ = 1.19×10-3 kg/s		Re=250, $\dot{m}_{in}$ =1.98×10-3 kg/s		Re=400, $\dot{m}_{in}$ = 3.17×10-3 kg/s	
		10^{-3} kg/s	%	10^{-3} kg/s	%	10^{-3} kg/s	%
L_2/D=2.50	$\dot{m}_{st}$	0.33	27.73	0.57	28.79	0.96	30.28
	$\dot{m}_{by}$	0.86	72.27	1.41	71.21	2.21	69.72
L_2/D=2.67	$\dot{m}_{st}$	0.35	29.41	0.60	30.30	1.00	31.55
	$\dot{m}_{by}$	0.84	70.59	1.38	69.70	2.17	68.45
L_2/D=3.33	$\dot{m}_{st}$	0.39	32.77	0.64	32.32	1.03	32.49
	$\dot{m}_{by}$	0.80	67.23	1.34	67.68	2.14	67.51
L_2/D=4.00	$\dot{m}_{st}$	0.41	34.45	0.67	33.84	1.06	33.44
	$\dot{m}_{by}$	0.78	65.55	1.31	66.16	2.11	66.56
L_2/D=5.00	$\dot{m}_{st}$	0.44	36.97	0.72	36.36	1.11	35.02
	$\dot{m}_{by}$	0.75	63.03	1.26	63.64	2.06	64.98
L_2/D=6.00	$\dot{m}_{st}$	0.46	38.66	0.75	37.88	1.15	36.28
	$\dot{m}_{by}$	0.73	61.34	1.23	62.12	2.02	63.72
L_2/D=6.67	$\dot{m}_{st}$	0.48	40.34	0.76	38.38	1.18	37.22
	$\dot{m}_{by}$	0.71	59.66	1.22	61.62	1.99	62.78

Table 5. Evaluation of the mass fluxes in the measure inlet section ($\dot{m}_{in}$) stenosis section ($\dot{m}_{st}$) and central bypass section ($\dot{m}_{by}$) for S = 75 %, α = 30° and D_1/D = 1 (with D = 3 mm).

		Re=150, $\dot{m}_{in}$ = 1.19×10-3 kg/s		Re=250, $\dot{m}_{in}$ =1.98×10-3 kg/s		Re=400, $\dot{m}_{in}$ = 3.17×10-3 kg/s	
		10^{-3} kg/s	%	10^{-3} kg/s	%	10^{-3} kg/s	%
L_2/D=2.50	$\dot{m}_{st}$	0.07	5.88	0.12	6.06	0.26	8.20
	$\dot{m}_{by}$	1.12	94.12	1.86	93.94	2.91	91.80
L_2/D=2.67	$\dot{m}_{st}$	0.07	5.88	0.11	5.56	0.20	6.31
	$\dot{m}_{by}$	1.12	94.12	1.87	94.44	2.97	93.69
L_2/D=3.33	$\dot{m}_{st}$	0.07	5.88	0.12	6.06	0.21	6.62
	$\dot{m}_{by}$	1.12	94.12	1.86	93.94	2.96	93.38
L_2/D=4.00	$\dot{m}_{st}$	0.08	6.72	0.13	6.57	0.22	6.94
	$\dot{m}_{by}$	1.11	93.28	1.85	93.43	2.95	93.06
L_2/D=5.00	$\dot{m}_{st}$	0.09	7.56	0.14	7.07	0.24	7.57
	$\dot{m}_{by}$	1.10	92.44	1.84	92.93	2.93	92.43
L_2/D=6.00	$\dot{m}_{st}$	0.10	8.40	0.16	8.08	0.25	7.89
	$\dot{m}_{by}$	1.09	91.60	1.82	91.92	2.92	92.11
L_2/D=6.67	$\dot{m}_{st}$	0.10	8.40	0.16	8.08	0.26	8.20
	$\dot{m}_{by}$	1.09	91.60	1.82	91.92	2.91	91.80

Table 6. Resistance R values for S = 50%.

	L_2/D	Δp/L [Pa]	$\dot{m}_{st}$ 10^{-3} [kg/s]	$\dot{m}_{by}$ 10^{-3} [kg/s]	R_{st} [Pa s / kg]	R_{by} [Pa s / kg]
Re=150	2.50	109.55	0.33	0.86	331970	127380
	2.67	109.46	0.35	0.84	312740	130310
	3.33	106.73	0.39	0.80	273670	133410
	4	102.42	0.41	0.78	249800	131310
	5	98.09	0.44	0.75	222930	130790
	6	91.71	0.46	0.73	199370	125630
	6.67	87.41	0.48	0.71	182100	123110
Re=250	2.50	202.39	0.57	1.41	355070	143540
	2.67	200.07	0.60	1.38	333450	144980
	3.33	197.79	0.64	1.34	309050	147600
	4	191.77	0.67	1.31	286220	146390
	5	182.89	0.72	1.26	254010	145150
	6	171.38	0.75	1.23	228510	139330
	6.67	162.02	0.76	1.22	213180	132800
Re=400	2.50	367.90	0.96	2.21	383230	166470
	2.67	367.90	1.00	2.17	367900	169540
	3.33	356.99	1.03	2.14	346590	166820
	4	349.56	1.06	2.11	329770	165670
	5	336.80	1.11	2.06	303420	163500
	6	318.20	1.15	2.02	276700	157520
	6.67	302.45	1.18	1.99	256310	151980

Table 7. Resistance R values for S = 75%.

	L_2/D	$\Delta p/L$ [Pa]	$\dot{m}_{st}$ 10^{-3} [kg/s]	$\dot{m}_{by}$ 10^{-3} [kg/s]	R_{st} [Pa s / kg]	R_{by} [Pa s / kg]
	2.50	118.50	0.07	1.12	169290	105800
	2.67	119.20	0.07	1.12	170290	106430
	3.33	118.13	0.07	1.12	168760	105470
Re=150	4	117.24	0.08	1.11	146550	105620
	5	115.87	0.09	1.10	128740	105340
	6	114.00	0.10	1.09	114000	104590
	6.67	112.38	0.10	1.09	112380	103100
	2.50	220.58	0.12	1.86	183820	118590
	2.67	219.39	0.11	1.87	199450	117320
	3.33	221.67	0.12	1.86	184720	119180
Re=250	4	219.44	0.13	1.85	168800	118620
	5	218.77	0.14	1.84	156260	118900
	6	217.09	0.16	1.82	135680	119280
	6.67	214.24	0.16	1.82	133900	117710
	2.50	403.70	0.26	2.91	201290	139970
	2.67	402.57	0.20	2.97	201280	135550
	3.33	405.40	0.21	2.96	193050	136960
Re=400	4	403.72	0.22	2.95	183510	136850
	5	403.98	0.24	2.93	168320	137880
	6	408.43	0.25	2.92	163370	139870
	6.67	407.32	0.26	2.91	156660	139970

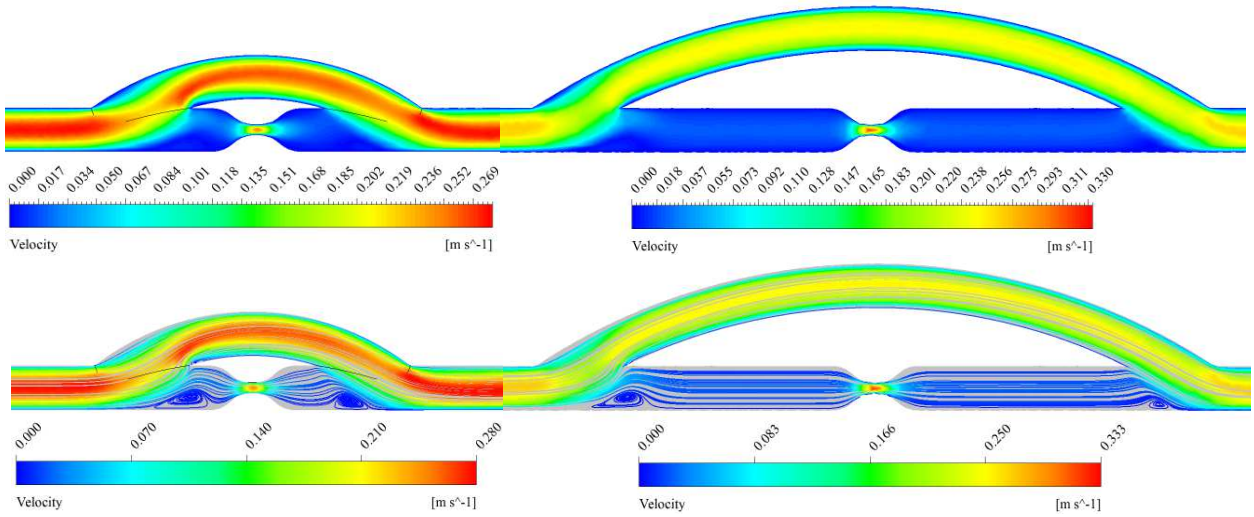

Fig. 9. Velocity contours (top) and streamlines (bottom) with reference to a couple of points having coordinates L_2/D=6.67, S=75%, Re=150 (right), and L_2/D=2.27, S=75%, and Re=150 (left).

4. Conclusions

In this work, the influence of the bypass attachment point L_2 from the artery stenosis position in different flow condition at fixed value of the junction angle α = 30° and diameter ratio D_1/D = 1 was studied. Three pressure drop trends for each stenosis degree were created using Constructal Design related to the CFD analysis. The considered stenosis degree S were equal to 50% and 75%. Instead, the Reynolds number Re were 150, 250 and 400. The obtained results showed a decrease in the pressure drop trend as the distance of the bypass attachment point increases. The decreasing pressure trend was less pronounced when S increases. Therefore, the optimum point is the point as far as possible from the shrinkage. The mass flows rate in the various sections of the system was evaluated. Moreover, the results showed that the flow was all the more diverted in the bypass section when the Reynolds number is more significant. It also computed the resistance flow values in the bypass and stenosis section. It is an alternative formulation for talking about the pressure drop trend. At this point, some limitations of this study should be mentioned. First of all, a steady-state condition was applied while the blood flow is known to be pulsating. Secondly, the blood was assumed as a Newtonian fluid, which may affect the results found at low Reynolds number. Moreover, the graft and arteries were assumed as rigid walls and idealized without considering a patient-specific vascular model. Besides, literature did not yet provide many experimental data that are essential for validation and clinical adoption of any proposed configuration. Despite the simplifications mentioned above and assumptions, by applying Constructal Design methodology, the main conclusions and the optimal graft design found in this paper followed previous studies that evaluated the graft design with other methodologies. Finally, we are strongly convinced that the employment of constructal design in hemodynamics here developed reinforces the versatility of Bejan's theory. It is worth mentioning that some promising applications of Constructal theory regard even nature [39,40] and renewable energy problems [41, 42]. This view of the field is unifying, the science and the applications together illustrate the evolutionary direction of the constructal law.

Author Contributions

Flavia Zinani and Luiz Rocha planned the scheme and initiated the project. Andrea Impiombato developed the mathematical modeling, conducted the simulations and examined the results validation. Cesare Biserni worked on the writing review and editing. The manuscript was written through the contribution of all authors. All authors approved the final version of the manuscript.

Conflict of Interest

The authors declared no potential conflicts of interest with respect to the research, authorship, and publication of this article.

Funding

The authors F.S.F. Zinani and L.A.O. Rocha are grant holders of CNPq (National Council for Scientific and Technological Development– Brasília – DF – Brazil), process numbers 307827/2018-6 and 307791/2019-0, respectively. The authors C. Biserni and A.N. Impiombato were sponsored by the Italian Ministry for Education, University and Research.

Nomenclature

D	Artery diameter [m]	D_0	Stenosis diameter [m]
D_1	Graft diameter [m]	D_{ij}	Strain rate tensor [s^{-1}]
L	Plane measure length [m]	L_1	Artery length [m]
L_2	Attachment point distance [m]	L_3	Stenosis beginning [m]
L_4	Graft length [m]	L_5	Inlet/outlet length [m]
N	Number of mesh elements [-]	$\tilde{p}$	Dimensionless pressure drop [-]
Pin	Pressure inlet [Pa]	P_{out}	Pressure outlet [Pa]
Re	Reynolds number [-]	S	Stenosis degree [-]
Um	Average velocity [m s^{-1}]	u_i	Velocity vector [m s^{-1}]
$\tilde{u}_i$	Dimensionless velocity field [-]	V	Artery volume [m^3]
V_1	Graft volume [m^3]	x_i	Position vector [m]
$\tilde{x}_i$	Dimensionless position vector [-]	α	Junction angle [deg]
ΔP	Pressure drop [Pa]	η	Viscosity function [Pa s]
μ	Dynamic viscosity [Pa s]	ρ	Mass density [kg m^{-3}]
γ	Shear rate [s^{-1}]	$\tilde{\tau}_{ij}$	Dimensionless extra-stress tensor [-]
τ_{ij}	Extra-stress tensor [Pa]		

References

[1] Ku, D.N., Giddens, D.P., Zarins, C.K., Glagov, S., Pulsatile Flow and Atherosclerosis in the Human Carotid Bifurcation, *Ateriosclerosis*, 5, 1985, 293 – 302.
[2] Tian, F.B., Zhu, L., Fok, P.W., Lu, X.Y., Simulation of a pulsatile non-Newtonian flow past a stenosed 2D artery with atherosclerosis, *Computers in Biology and Medicine*, 43(9), 2013, 1098 - 1113.
[3] Liu, G., Wu, J., Ghista, D.N., Huang, W., Wong, K.K., Hemodynamic characterization of transient blood flow in right coronary arteries with varying curvature and side-branch bifurcation angles, *Computers in Biology and Medicine*, 64, 2015, 117 – 126.
[4] Guerciotti, B., Vergara, C., Ippolito, S., Quarteroni, A., Antona, C., Scrofani, R. A., Computational fluid-structure interaction analysis of coronary Y-grafts, *Medical Engineering & Physics*, 47, 2017, 117 - 127.
[5] Bassiouny, H.S., White, S., Glagov, S., Choi, E., Giddensc, D.P., Zarins, C.K., Anastomotic intimal hyperplasia: mechanical injury or flow induced, *Journal of Vascular Surgery*, 15(4), 1992, 708 – 717.
[6] Bertolotti, C., Deplano, V., Fuseri, J., Dupouy, P., Numerical and experimental models of post-operative realistic flows in stenosed coronary bypasses, *Journal of Biomechanics*, 34(8), 2001, 1049 – 1064.
[7] Lee, D., Su, J., Liang, H., A numerical simulation of steady flow fields in a bypass tube, *Journal of Biomechanics*, 34(11), 2001, 1407 – 1416.
[8] Vimmr, J., Jonášová, A., Non-Newtonian effects of blood flow in complete coronary and femoral bypasses, *Mathematics and Computers in Simulation*, 80(6), 2010, 1324 – 1336.
[9] Koksungnoen, S., Rattanadecho, P., Wongchadakul, P., 3D numerical model of blood flow in the coronary artery bypass graft during no pulse and pulse situations: Effects of an anastomotic angle and characteristics of fluid, *Journal of Mechanical Science and Technology*, 32, 2018, 4545–4552.
[10] Ballarin, F., Faggiano, E., Manzoni, A., Quarteroni, A., Rozza, G., Ippolito, S., Antona, C., Scrofani, R., Numerical modeling of hemodynamics scenarios of patient-specific coronary artery bypass grafts, *Biomechanics and Modeling in Mechanobiology*, 16, 2017, 1373–1399.
[11] Kabinejadian, F., Ghista, D.N., Compliant model of a coupled sequential coronary arterial bypass graft: Effects of vessel wall elasticity and non-Newtonian rheology on blood flow regime and hemodynamic parameters distribution, *Medical Engineering & Physics*, 34, 2012, 860– 872.
[12] O'Callaghan, S., Walsh, M., McGloughlin, T., Numerical modelling of Newtonian and non-Newtonian representation of blood in a distal end-to-side vascular bypass graft anastomosis, *Medical Engineering & Physics*, 28, 2006, 70–74.
[13] Ku, J.P., Elkins, C.J., Taylor, C.A., Comparison of CFD and MRI Flow and Velocities in an In Vitro Large Artery Bypass Graft Model, *Annals of Biomedical Engineering*, 33, 2005, 257–269.
[14] Bonert, M., Myers, J.G., Fremes, S., Williams, J., Ethier, C.R., A Numerical Study of Blood Flow in Coronary Artery Bypass Graft Side-to-Side Anastomoses, *Annals of Biomedical Engineering*, 30, 2002, 599–611.
[15] Dutra, R.F., Zinani, F.S., Rocha, L.A.O., Biserni, C., Constructal design of an arterial bypass graft, *Heat Transfer*, 49, 2020, 4019-4039.
[16] Troina G., Cunha M.L., Pinto, V.T., Rocha, L.A.O., Dos Santos, E.D., Fragassa, C., Isoldi, L.A., Computational Modeling and Constructal Design Theory Applied to the Geometric Optimization of Thin Steel Plates with Stiffeners Subjected to Uniform Transverse Load, *Metals*, 10, 2020, 220 – 249.
[17] Amaral, R.R., Troina, G.S., Fragassa, C., Pavlovic, A., Cunha, M.L., Rocha, L.A.O., Dos Santos, E.D., Isoldi, L.A., Constructal design method dealing with stiffened plates and symmetry boundaries, *Theoretical and Applied Mechanics Letters*, 10, 2020, 366 - 376.
[18] Bejan, A., *Advanced Engineering Thermodynamics*. 2nd ed, John Wiley & Sons, New York, 1997.
[19] Bejan, A., *Advanced Engineering Thermodynamics*, John Wiley & Sons, New York, 2016.
[20] Bejan, A., Lorente, S., *Design with Constructal Theory*, John Wiley & Sons, New York, 2008.
[21] Reis, A.H., Constructal theory: from engineering to physics, and how flow systems develop shape and structure, *ASME Appplied Mechanics Reviews*, 59, 2006, 269-282.
[22] Bejan, A., Lorente, S., The constructal law and the evolution of design in nature, *Physics of Life Reviews*, 8, 2011, 209 – 240.
[23] Chen, L., Progress in study on constructal theory and its applications, *Science China Technological Sciences*, 55(3), 2012, 802 – 820.
[24] Rocha, L.A.O., Lorente, S., Bejan, A., Constructal theory in heat transfer, *Handbook of Thermal Science and Engineering*, Springer International Publishing, Cham, 2017.
[25] Razera, A.L., da Fonseca, R.J.C., Isoldi, L.A., dos Santos, E.D., Rocha, L.A.O., Biserni, C., Constructal design of a semi-elliptical fin inserted in a lid-driven square cavity with mixed convection, *International Journal of Heat and Mass Transfer*, 126, 2018, 81 - 94.
[26] Fagundes, T., Lorenzini, G., Estrada, E. da S.D., Isoldi, L.A., dos Santos, E.D., Rocha, L.A.O., da Silva, N. A., Constructal design of conductive asymmetric tri-forked pathways, *Journal of Engineering Thermophysics*, 28(1), 2019, 26 – 42.
[27] Wang, H., Dai, W., Bejan, A., Optimal temperature distribution in a 3D triple-layered skin structure embedded with artery and vein vasculature and induced by electromagnetic radiation, *International Journal of Heat and Mass Transfer*, 50(9,10), 2007,1843 – 1854.
[28] Lucia, U., Grisolia, G., Constructal law and ion transfer in normal and cancer cells, *Proc. Romanian Academy-Special Issue*, 2018, 213—218.

[29] Politis, A.K., Stavropoulos, G.P., Christolis, M.N., Panagopoulos, F.G., Vlachos, N.S., Markatos, N.C., Numerical modeling of simulated blood flow in idealized composite arterial coronary grafts: Steady state simulations, *Journal of Biomechanics*, 40, 2007, 1125-1136.
[30] Johnston, B.M., Johnston, P.R., Corney, S., Kilpatrick, D., Non-Newtonian blood flow in human right coronary arteries: steady state simulations, *Journal of Biomechanics*, 37, 2004, 709-720.
[31] Ko, T., Ting, K., Yeh, H., Numerical investigation on flow fields in partially stenosed artery with complete bypass graft: An in vitro study, *International Communications in Heat and Mass Transfer*, 34(6), 2007, 713 – 727.
[32] Ko, T., Ting, K., Yeh, H., A numerical study on the effects of anastomotic angle on the flow fields in a stenosed artery with a complete bypass graft, *International Communications in Heat and Mass Transfer*, 35(10), 2008, 1360 – 1367.
[33] Xiong, F., Chong, C., A parametric numerical investigation on haemodynamics in distal coronary anastomoses, *Medical Engineering & Physics*, 30(3), 2008, 311 – 320.
[34] Bejan, A., *Convection Heat Transfer*, John Wiley & Sons, New York, 2013.
[35] Slattery, J.C., *Advanced Transport Phenomena*, Cambridge University Press, 1999.
[36] ANSYS, *Ansys Fluent User's Guide*, Canonsburg, 2015.
[37] Baliga, B., Patankar, S., A new finite-element formulation for convection-diffusion problems, *Numerical Heat Transfer*, 3(4), 1980, 393 – 409.
[38] Celik, I.B., Ghia, U., Roache, P. J., Freitas, C. J., Coleman, H., Raad, P. E., Procedure for estimation and reporting of uncertainty due to discretization in CFD applications, *Journal of Fluids Engineering*, 130, 2008, 078001-4.
[39] Bejan, A., Lorente, S., Lee, L., Unifying constructal theory of tree roots, canopies and forests, *Journal of Theoretical Biology*, 254, 2008, 529–540.
[40] Bejan, A., Lorente, S., Constructal theory of generation of configuration in nature and engineering, *Journal of Applied Physics*, 100, 2006, 041301.
[41] Vieira, R.S., Petry, A.P., Rocha, L.A.O., Isoldi, E.D., Dos Santos, E.D., Numerical evaluation of a solar chimney geometry for different ground temperatures by means of constructal design, *Renewable Energy*, 109, 2017, 222–234.
[42] Martins, J.C., Goulart, M.M., Gomes, M.N., Souza, J.A., Rocha, L.A.O., Isoldi, L.A., Dos Santos, E.D., Geometric Evaluation of the Main Operational Principle of an Overtopping Wave Energy Converter by Means of Constructal Design, *Renewable Energy*, 118, 2018, 727–741.

ORCID iD

Andrea Natale Impiombato https://orcid.org/0000-0003-1103-8058
Flavia Schwarz Franceschini Zinani https://orcid.org/0000-0001-5402-900X
Luiz Alberto Oliveira Rocha https://orcid.org/0000-0003-2409-3152
Cesare Biserni https://orcid.org/0000-0003-0081-2036

How to cite this article: Impiombato A.N., Franceschini Zinani F.S., Oliveira Rocha L.A., Biserni C. Constructal Design of an Idealize Arterial Bypass Graft: Effect of the Bypass Attachment Pointon Resistance to Flow, *J. Appl. Comput. Mech.*, 7(1), 2021, 334–344. https://doi.org/10.22055/JACM.2020.35246.2607